Asian Journal of Chemistry; Vol. 32, No. 11 (2020), 2887-2892

ASIAN JOURNAL OF CHEMISTRY

https://doi.org/10.14233/ajchem.2020.22872

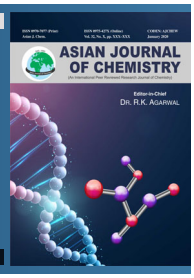

Synthesis, Thermal and Antimicrobial Activity of Novel Organic Single Crystal of (*E*)-4-Bromo-2-[(phenylimino)methyl]phenol Compound

R. IDAMALARSELVI[1,*], G. SWETHA[1], C. RAMACHANDRA RAJA[2] and R. PRISCILLA[3]

[1]Department of Physics, D.G. Government Arts College for Women (Affiliated to Bharathidasan University, Tiruchirappalli), Mayiladuthurai-609001, India
[2]Department of Physics, Government Arts College (Autonomous) (Affiliated to Bharathidasan University, Tiruchirappalli), Kumbakonam-612001, India
[3]Department of Physics, A.D.M. College for Women (Autonomous) (Affiliated to Bharathidasan University, Tiruchirappalli), Nagapattinam-611001, India

*Corresponding author: E-mail: idamalarselvi@gmail.com

Received: 25 June 2020; *Accepted*: 19 August 2020; *Published online*: 28 October 2020; AJC-20113

This study focused on kinetic modelling of a specific type of multistep heterogeneous reaction comprising exothermic and endothermic reaction steps, as exemplified by the experimental kinetic curves for the thermal decomposition of (*E*)-4-bromo-2-[(phenylimino)methyl]-phenol (4B2PMP) crystal. The crystal was grown by a slow evaporation method. The cell parameters and crystalline perfection of the grown crystal were studied by single and powder X-ray diffractions. Thermal stability and phase change of 4B2PMP crystal were analyzed by TG/DTA. The microhardness study has revealed the soft nature. UV-visible analysis reveals the wide range of optical window of the optical transmission from 199 nm to 1100 nm. The bandgap of the crystal is found to be 3.24 eV. The FESEM of the crystals was spherically shaped and consisted of a core-shell structure with internal aggregates. The antimicrobial activity of title crystal was tested against different microorganisms by disc diffusion method. The results reveal that the title compound have effective antimicrobial activities.

Keywords: (*E*)-4-Bromo-2-[(phenylimino)methyl]phenol, Crystal structure, Kinetic deconvolution analysis.

INTRODUCTION

Kinetic analysis of various reaction processes using various thermoanalytical techniques is widely applied in a different field with various purpose. Thermoanalytical approaches to the heterogeneous multistep reactions. However, further complications are introduced when the overall response comprises partially overlapping processes with oppositely signed thermoanalytical signals (*e.g.*, mass loss/gain or exothermic and endothermic events) [1-4].

From the viewpoint of the overall thermal effect revealed that using DSC, the reaction starts as an endothermic reaction due to the overall decomposition of (*E*)-4-bromo-2-[(phenylimino)methyl]phenol (4B2PMP) crystal and becomes the exothermic evaporation/decomposition of the *in situ* produced residual mass of the crystal [5,6]. This study focuses on the establishment of a methodology for kinetic modelling of an overall reaction into exothermic and endothermic steps using simultaneously recorded TG and DSC curves. The results of kinetic analysis, including the contribution of each reaction step to the overall reaction, are refined by assuming that the kinetic data/for overall reaction process is the sum of the two reaction steps weighted by the contribution of each reaction steps. Furthermore, strategies for further detailed phenomenological kinetic characterization. Also, the physico-chemical kinetic interpretation of mechanical, optical, elastic, microstructure is discussed by reviewing the results of the practical kinetic analysis of the experimental TG-DSC curves for the thermal decomposition of the crystal 4B2PMP.

Yan *et al.* [7] reported the crystal structure of 2-(*E*)-(4-bromophenyl)iminomethyl]-4-chlorophenol. The crystal structure has been analyzed in terms of rigid-body motion, molecular shape, packing arrangement and bond length were discussed. Muravyev *et al.* [8] reported the kinetic modelling of a specific

type of multistep heterogeneous reaction comprising exothermic and endothermic reaction steps, as exemplified by the practical kinetic analysis of the experimental kinetic curves for the thermal decomposition of molten ammonium dinitramide (ADN). Nakano *et al*. [9] reported the kinetic modelling of the thermal decomposition of sodium percarbonate (sodium carbonate-hydrogen peroxide (2/3)). The reaction is characterized by apparently different kinetic profiles of mass-loss and exothermic and endothermic behaviour as recorded by TG/DSC analysis.

The concept about the levels of structure is developed, which include the concept in equilibrium and kinetics, the geometry of a crystal, the arrangement of atoms in the unit cell of crystalline material, the microstructure of the material. The novelty of the work focuses on the establishment of a methodology for kinetic modelling of an overall reaction into exothermic and endothermic steps using simultaneously recorded TG and DSC curves [10-12]. The synthesized 4B2PMP crystal was primarily parted for their *in vitro* growth constraint activity against a different strain of bacterial and fungal.

EXPERIMENTAL

The chemicals *viz*. 5-bromo-2-hydroxybenzaldehyde and aniline used in the present work were of analytical reagent (AR) with a minimum assay of 99% and obtained from E-Merck, Germany.

Synthesis of (*E*)-4-bromo-2-[(phenylimino)methyl]-phenol (4B2PMP) crystal: 5-Bromosalicylaldehyde (0.4g, 0.004 mol) was dissolved in a mixture of CCl_4 (5 mL) and DMSO (5 mL). To this solution, aniline (0.372 g, 0.0035mol) was added dropwise with constant stirring for 1 h and the solution turned deep yellow. On standing for 1 week and with slow evaporation of solvent, orange crystal is obtained.

Antimicrobial activities: The antimicrobial activities of 4B2PMP crystal were analyzed by the disk diffusion method. Test pathogens (*E. lenta*, *S. epidermis*, *B. substilis*, *S. mutans*, *E. faecalis*, *K. pneumoniae*, *P. aeruginosa*, *E. coli*, *C. albicans* and *A. niger*) were spread on Mueller-Hinton agar (MHA) plates. A well of diameter 6 mm was made using a sterile cork borer and loaded with a required concentration of drug over the agar. The test plates were incubated for 24 h at 37 ºC. The zone of inhibition (mm in diameter) was taken as the activity against the test pathogens.

RESULTS AND DISCUSSION

XRD analysis: The synthesized (*E*)-4-bromo-2-[(phenylimino)methyl]-phenol (4B2PMP) crystal was subjected to single crystal X-ray diffraction (SXRD) analysis using Bruker AXS Kappa APEX-II single-crystal X-ray diffractometer, equipped with graphite monochromated Mo*K*α radiation (λ = 0.710 Å) at room temperature. The single-XRD analysis (Fig. 1a) confirmed that the grown crystal belongs to the orthorhombic crystal system with the space group of $Pca2_1$ (Table-1) [13].

TABLE-1
COMPARISON OF POWDER AND SINGLE XRD DATA FOR 4B2PMP CRYSTAL

Molecular formula	$C_{13}H_{10}BrNO$	
Molecular weight	276.13 g/mol	
Crystal system, space group	Orthorhombic, $Pca2_1$	
Unit cell	Single XRD	Powder XRD at 200 °C
a (Å)	12.353 Å	12.567 Å
b (Å)	4.5092 Å	4.876 Å
c (Å)	19.778 Å	19.191 Å
α	90°	90°
β	90°	90°
γ	90°	90°
Volume (Å^3)	1107 Å^3	1101 Å^3

Powder X-ray diffraction analysis: The grown 4B2PMP crystal was subjected to PXRD analysis using Cu*K*α (λ = 1.54060 Å) radiation with the help of pan analytical Xpert-pro X-ray diffractometer in the 2θ values ranging from 10º to 80º. Ind X software was used to index the corresponding peaks. Fig. 1b shows the diffraction profile peaks of 4B2PMP sample calcined at 300 ºC for 3 h with promise pure orthorhombic crystal system for the 4B2PMP powder with the space $Pca2_1$. It is pure from the diffraction pattern of the crystalline in nature. The sample shows major peak assigned to the 21.643º of the peak 2θ values 14.305º and 35.194º with interplan of spacing corresponding to diffraction planes of 2 0 0, 0 1 2, 1 1 4 and 4 1 0 (Table-1). The thermally induced growth mechanisms each to increase in the grain size, which may be due to the reduce FWHM value (Table-2). Determination of density in dislocation crystal explain the defect the unit volume of the sample.

Thermoanalytical measurements: Thermal studies with crystals can predict a product's performance and thermal history

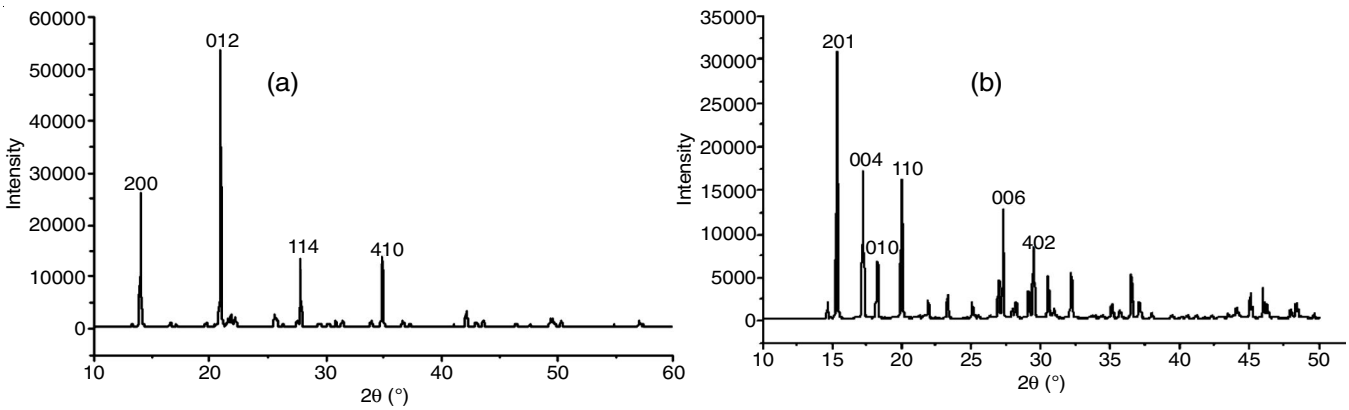

Fig. 1. (a) High temperature, (b) Room temperature powder XRD spectrum of 4B2PMP

TABLE-2
STRUCTURAL PARAMETERS OF POWDER XRD FOR 4B2PMP CRYSTAL

Sample	2θ (°)	h k l	FWHM	Crystallize size (D) (nm)	Dislocation density (δ)
5BSA (RT)	15.358	2 0 0	0.23	3.5223	8.06
5BSA (HT-300 °C)	21. 643	2 0 2	0.06	12.31	6.60

of the sample in uses *i.e.* its thickness, stability, melting point, crystal perfection, orientation and phase transition which can be accurately measured. The % of weight loss data (TG curve) from a 3.332 mg sample run under vacuum and with the analysis of nitrogen gas showed the loss of -90.21% at 420 ºC (1st weight loss) and a slow loss of -91.93% (2nd weight loss) starting around 489 ºC. The sample was measured for its real density and the resulting data are shown on the DTA curve, undoubtfully the sharp exotherm at 325.6 ºC represents a phase change (Fig. 2). DSC thermogram indicates the exothermic and endothermic patterns. The first sharp endotherm at 123.1 ºC is an indicative of the heat capacity enthalpy of crystallization. Second sharp exotherm at 333.5 ºC is due to the enthalpy of melting. Exothermic behaviour (without decomposition) was chemically associated with the decreasing enthalpy. Narrow exotherm usually indicates crystallization (orderly) of a metastable system, which is directly proportional to the amount of heat energy disrobed by the sample. The negative values of enthalpy referred to the chemical bond formed and heat is released. This study focused on kinetic modelling of a specific type of multistep heterogeneous reaction comprising exothermic in signal step and endothermic reaction step, as exemplified by the practical kinetic analysis of the experimental kinetic curves for the thermal decomposition of 4B2PMP crystal.

The important result of the present kinetic approach of separating the exothermic and endothermic reaction steps of thermal decomposition of 4B2PMP is that the net thermal effect of each reaction step, Q1 and Q2 and the relationship of these net thermal effects to the gross thermal effects. The $Q_{\Sigma} = 1133.35$ J of the overall reaction process, can be estimated using the kinetic parameters. To evaluate the thermal anomaly of the crystal, the enthalpy of fusion (ΔH_f), entropy of fusion (ΔS_f), Gibbs free energy (ΔG_f), activation energy (E_a), thermal conductivity (w), heat capacity and specific heat capacity (C_p) were measured (Table-3). The specific heat capacity displays abrupt change due to the implementation of the configurational

TABLE-3
THERMODYNAMICAL DATA FOR 4B2PMP SINGLE CRYSTAL

Phase transition	325.6 °C	
Enthalpy of fusion ΔH_f (kJ mol^{-1})	73.67	
Entropy of fusion ΔS_f (J k^{-1}mol^{-1})	0.5984	
Gibbs free energy ΔG_f (Jk^{-1}mol^{-1})	21953	
Activation energy E_a^c (kJmol^{-1})	232.7	
Specific heat capacity (Cp) J/g ºC	1.40 - Endo	4.48 Exo
Heat capacity (Q) J	471.68 - Endo	-2895.2 - Exo

degree of kinetic freedom of rotational and atom transfer. In the system, heat is absorbed and realized simultaneous due to positive and negative enthalpy reactions [14-23].

Activation energy: An Arrhenius method is used to measure the activation energy of the phase transition. The value obtained for the phase change in high-temperature is $E_a = 232.7$ kJ/mol. This represents the adequate energy that stimulates both nucleation and development. Activation energy associated with each stage of decomposition is described by the equation.

$$\ln\left[\ln\left(\frac{1}{y}\right)\right] = \left(-\frac{E_a}{R}\right)\frac{1}{T} + \text{Constant}$$

Mechanical stability and elastic properties: The hardness of the crystal and the elastic properties such as young, bulk and shear module were calculated at a particular temperature. The experiment was carried out in the load range from 5 to 50 g over a fixed interval time of 5 s. The indentation patterns were measured by the optical microscope. The hardness number (H_v) was calculated using the following standard eqn.:

$$H_V = 1.8544X\left(\frac{P}{d^2}\right)\text{Kg/mm}^2$$

where P is the applied load and d is the diagonal length.

It is shown that the hardness number increases upto 50 g and then decreases with increasing load Fig. 3a. It may be due to the reverse indentation size effect (RISE) and it is attributed

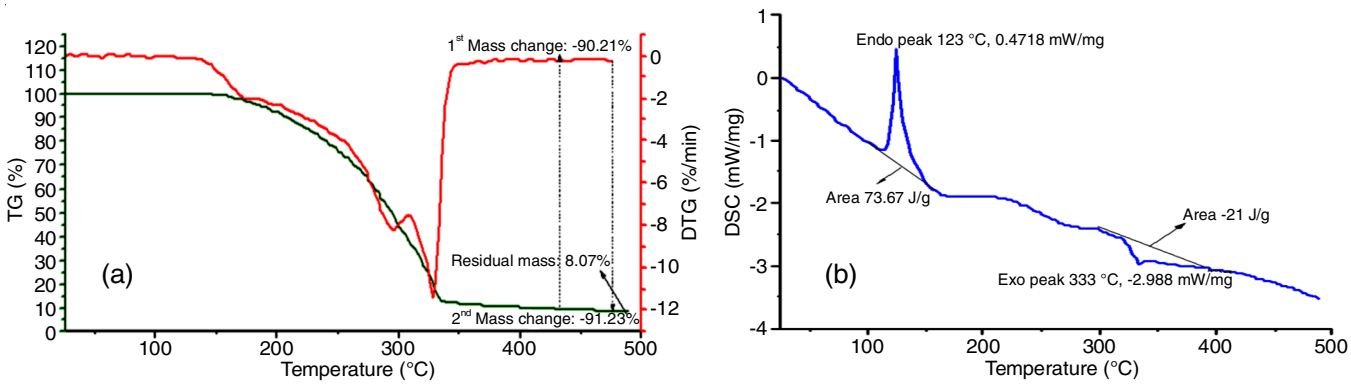

Fig. 2. (a) TG -DTA curve and (b) DSC curve of 4B2PMP

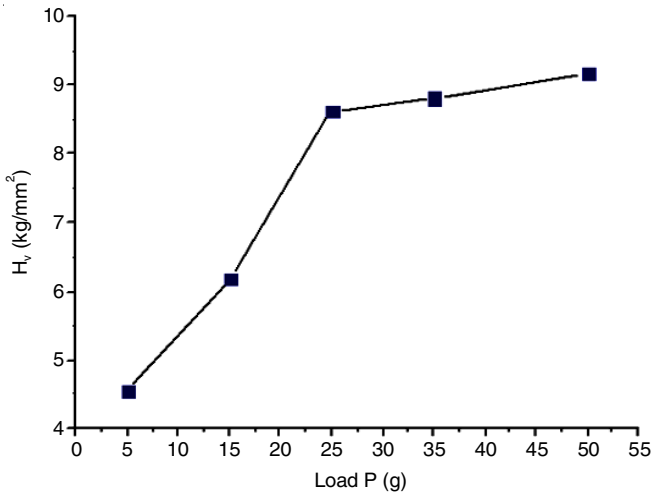

Fig. 3a. Vickers microhardness spectrum of 4B2PMP single crystal with applied load

to the predominance of nucleation, the existence of distorted zone near the crystal interface, an effect of vibrations, specimen chipping around the indentation, radial cracks and multiplication of dislocations of the sample. The maximum hardness number of the grown crystal was found to be 9.18 kg/mm^2 and it evidences good mechanical stability (Table-4).

$$P = Kd^n$$

$$\log P = \log K + n \log$$

where P is the applied load (g); d is the diameter of recovered indentation (mm) and K is the material constant. The Meyer's graph was plotted between log P *versus* log d (Fig. 3b) and it provides the straight line and works hardening coefficient (n) is assessed from the slope. The n value is determined to be 2.97, which is higher than 2, reveals the soft nature of 4B2PMP.

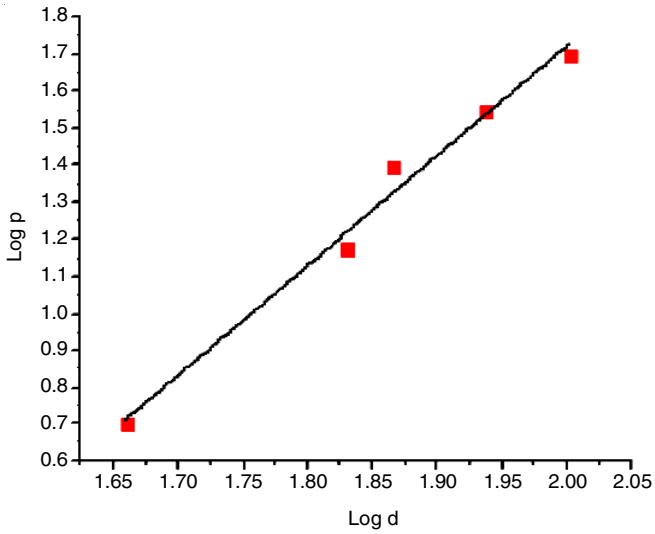

Fig. 3b. Plot of log P *vs.* log d of 4B2PMP crystal

UV-Vis analysis: The optical study was performed using UV-vis/NIR spectrophotometer (Perkin-Elmer Lambda 35). UV visible spectra obtained for representative 4B2PMP crystal from 199 nm to 1100 nm. The absorption spectrum in Fig. 4 shows a lower cut off wavelength 346 nm at room temperature and 350 nm at 300 ºC. 4B2PMP crystal is said to exhibit π-π*

TABLE-4
MECHANICAL AND ELASTIC DATA OF 4B2PMP CRYSTAL

Vickers hardness (H_v)	Stress (σ)	Strain (ε)	Young's modulus E (N/m^2)	Bulk modulus B (N/m^2)	Shear modulus G (N/m^2)
4.53	0.109	0.171	0.640	0.1576	0.361
6.18	0.221	0.071	3.110	0.767	1.757
8.62	0.340	0.043	7.839	1.933	4.429
8.82	0.404	0.043	9.292	2.292	5.250
9.18	0.497	0.040	12.41	3.062	7.014

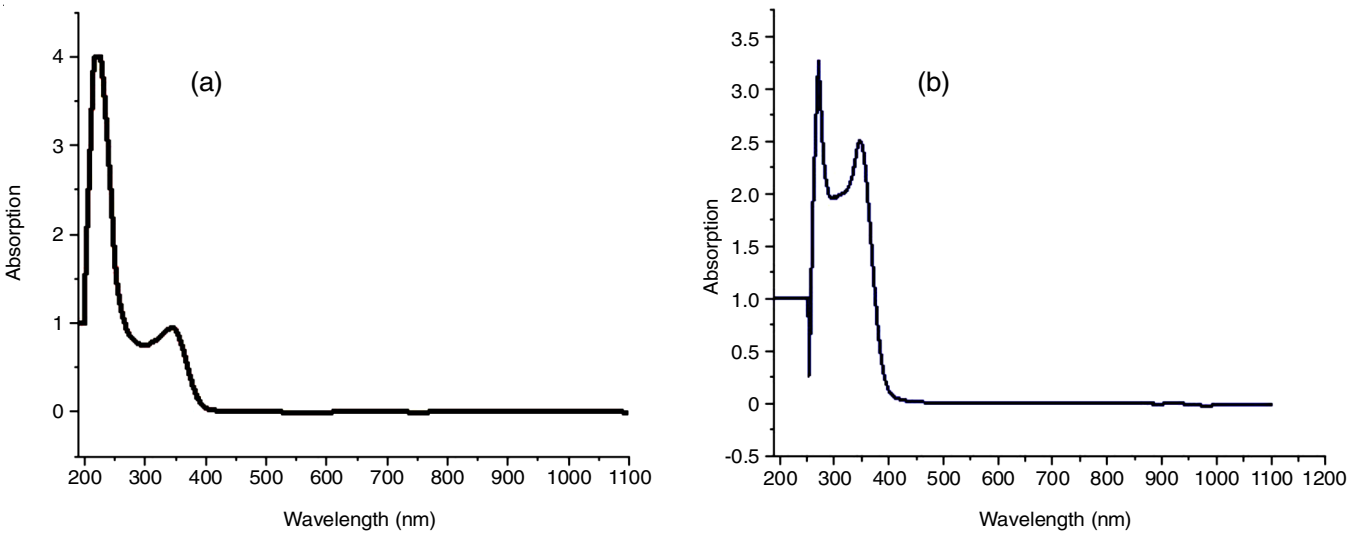

Fig. 4. UV-visible absorption spectrum of 4B2PMP crystal at room temperature (a) and 300 ºC (b)

transition [24,25]. The transmittance (T) of 4B2PMP crystal is used to determine the general equation:

$$\text{Energy (E)} = \frac{\text{Planks constant (h)} \times \text{Speed of light (c)}}{\text{Wavelength } (\lambda)}$$

where, energy (E) = Bandgap, Plank's constant (h) = 6.626×10^{-34} J/s, velocity of light (c) = 2.99×10^{8} m/s and wavelength (λ) = absorption peak value, also 1 eV = 1.6×10^{-19}.

The linear part is extrapolated and intercept in x coordinates and the band value wass found to be 3.61 eV at room temperature and 3.57 eV at 300 °C. This high-temperature band gap to the optical colour changed in the transparency of the crystal is especially suited for the thermochromic application.

FESEM-EDAX analysis: The shape, size and distribution of the crystal, as prepared composite sample and microstructure were examined using a super 55 CARL ZEISS FESEM-EDAX. Fig. 5 shows the field scanning electron microscopic images of the 4B2PMP crystal, which reflects that crystals were spherically shaped and consisted of a core-shell structure with internal aggregates of 4B2PMP crystalline particles radiating from the centre and covered by a surface layer composed of 4B2PMP crystalline particles. The molar fraction of $C_{13}H_{10}NOBr$ in 4B2PMP crystals used in the present study was calculated to be 7.37 ± 1.37 mol% from the mass loss value during the thermal decomposition of 4B2PMP crystal [26].

The elemental analysis was carried out by EDAX for the 4B2PMP crystal, the average atomic percentage and weight percentage are shown. From the weight% bar chart, it was evident that the major component of the crystal mixture. The content varied in the order C > Br > O > Al by which the component was mixed experimentally.

Antimicrobial studies: The MIC values (Table-5) specified that the synthesized 4B2PMP crystal exhibited a promising results compared to the ligand against tested microorganisms (*E. lenta*, *S. epidermis*, *B. substilis*, *S. mutans*, *E. faecalis*, *K. pneumoniae*, *P. aeruginosa*, *E. coli*, *C. albicans* and *A. niger*). An enhancement in the activity may be efficient on the basis that ligands mainly possess C=N bond. The outcome of antimicrobial activity evaluation of the synthesized compounds revealed that the synthesized 4B2PMP compound possessed antibacterial and antifungal activities. The 4B2PMP compound displayed moderate antibacterial activity at MIC = 50 and 250 µg/mL and good antifungal activity at MIC= 50 µg/mL against tested bacteria and fungi, respectively.

Conclusion

A novel organic material (*E*)-4-bromo-2-[(phenylimino)-methyl]phenol (4B2PMP) was synthesized with improved heat

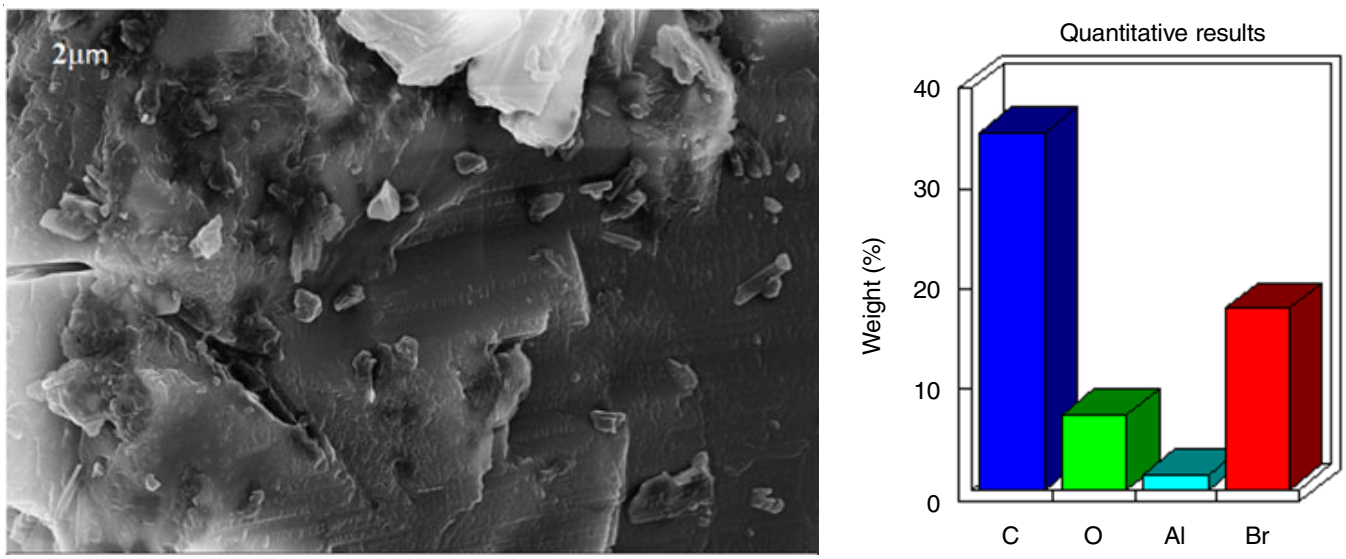

Fig. 5. FESEM micrograph and weight percentage of 4B2PMP corresponds to the different scale bar

TABLE-5
ANTIMICROBIAL ACTIVITIES OF 4B2PMP CRYSTAL

Strain	50 µg	100 µg	250 µg	500 µg	Positive control
E. lenta	–	11 mm	12 mm	14 mm	34 mm
S. epidermis	9 mm	11 mm	14 mm	17 mm	30 mm
B. substilis	11 mm	12 mm	13 mm	15 mm	33 mm
S. mutans	–	–	–	13 mm	41 mm
E. faecalis	–	–	12 mm	14 mm	32 mm
K. pneumoniae	–	–	–	10 mm	32 mm
P. aeruginosa	–	–	10 mm	12 mm	31 mm
E. coli	–	–	–	18 mm	42 mm
C. albicans	–	12 mm	14 mm	22 mm	21 mm
A. niger	14 mm	21 mm	25 mm	26 mm	17 mm

resistant, mechanical and high thermal stability being self extinguishable property. The thermochromic application kinetic modelling for the thermal decomposition of 4B2PMP crystal was applied to the multistep reactions which involve both endothermic and exothermic processes as the component reactions. These include the oxidative deterioration of solids and the thermal decomposition of oxidizing solids. The antimicrobial activities of the organic material were also performed by disk diffusion method and the result revealed that the organic crystals have effective antimicrobial activities.

ACKNOWLEDGEMENTS

The authors gratefully acknowledge SAIF, IIT Madras, Chennai, India, for SXRD, PXRD, TG-DTA/ DSC, UV-Vis NIR, Vicker′s Microhardness analyses and International Research Centre, Sathyabama University, Chennai, India for FESEM-EDAX analysis.

CONFLICT OF INTEREST

The authors declare that there is no conflict of interests regarding the publication of this article.

REFERENCES

1. G. Tan, Q. Wang, H. Zheng, W. Zhao, S. Zhang and Z. Liu, *J. Phys. Chem. A*, **115**, 5517 (2011); https://doi.org/10.1021/jp203580r
2. S. Vyazovkin and C.A. Wight, *Chem. Mater.*, **11**, 3386 (1999); https://doi.org/10.1021/cm9904382
3. A.K. Galwey, *J. Therm. Anal. Calorim.*, (2020) (In press); https://doi.org/10.1007/s10973-020-09461-w
4. S.Vyazovkin, A.K. Burnham, L. Favergeon, N. Koga, E. Moukhina, L.A. Pérez-Maqueda and N. Sbirrazzuoli, *Thermochim. Acta*, **689**, 178597 (2020); https://doi.org/10.1016/j.tca.2020.178597
5. G. Sanders and P.K. Gallagher, *Thermochim. Acta*, **388**, 115 (2002); https://doi.org/10.1016/S0040-6031(02)00032-1
6. G. Garcia-Garrido, P.E. Sánchez-Jiménez, L.A. Pérez-Maqued, A. Perejón and J.M. Criado, *Phys. Chem. Chem. Phys.*, **18**, 29348 (2016); https://doi.org/10.1039/C6CP03677E
7. X.-X. Yan, L.-P. Lu and M.-L. Zhu, *Acta Cryst.*, **E70**, o853 (2014); https://doi.org/10.1107/S1600536814015268
8. N.V. Muravyev, N. Koga, D.B. Meerov and A.N. Pivkina, *Phys. Chem. Chem. Phys.*, **19**, 3254 (2017); https://doi.org/10.1039/C6CP08218A
9. M. Nakano, T. Wada and N. Koga, *J. Phys. Chem. A*, **119**, 9761 (2015); https://doi.org/10.1021/acs.jpca.5b07044
10. C.G. Hamaker, O.S. Maryashina, D.K. Daley and A.L.J. Wadler, *Chem. Cryst.*, **40**, 34 (2010); https://doi.org/10.1007/s10870-009-9601-5
11. N. Dege, M.S.H. Faizi, O.E. Dogan, E. Agar and I.A. Golenya, *Cryst. Commun.*, **75**, 770 (2019); https://doi.org/10.1107/S205698901900642X
12. S.-S. Qian, Y.-T. Ye, J.-Q. Ren, Z. You and H.-L. Zhu, *Synth. React. Inorg. Met.-Org. Nano-Metal Chem.*, **46**, 1220 (2016); https://doi.org/10.1080/15533174.2015.1004449
13. S. Leela, T.D. Rani, A. Subashini, S. Brindha, R.R. Babu and K. Ramamurthi, *Arab. J. Chem.*, **10**, S3974 (2017); https://doi.org/10.1016/j.arabjc.2014.06.008
14. T. Taniguchi, H. Sato, Y. Hagiwara, T. Asahi and H. Koshima, *Commun. Chem.*, **2**, 19 (2019); https://doi.org/10.1038/s42004-019-0121-8
15. V.K. Gupta and R.A. Singh, *RSC Adv.*, **5**, 38591 (2015); https://doi.org/10.1039/C5RA04907E
16. P. Karuppasamy, T. Kamalesh, V. Mohankumar, S.A. Kalam, M.S. Pandian, P. Ramasamy, S. Verma and S.V. Rao, *J. Mol. Struct.*, **1176**, 254 (2019); https://doi.org/10.1016/j.molstruc.2018.08.074
17. M.V. Kök and E. Okandan, *J. Therm. Anal.*, **46**, 1657 (1996); https://doi.org/10.1007/BF01980771
18. M. Magesh, G.A. Babu and P. Ramasamy, *J. Cryst. Growth*, **324**, 201 (2011); https://doi.org/10.1016/j.jcrysgro.2011.03.057
19. M.S. Kumar, K. Rajesh, G.V. Vijayaraghavan and S. Krishnan, *Mater. Sci. Pol.*, **36**, 733 (2018); https://doi.org/10.2478/msp-2018-0086
20. H. Liu, H. Wu, H. Yu, Z. Hu and Y. Wu, *Dalton Trans.*, **48**, 16626 (2019); https://doi.org/10.1039/C9DT03451J
21. S. Sudhahar, M.K. Kumar, A. Silambarasan, R. Muralidharan and R.M. Kumar, *J. Mater.*, **7**, 539312 (2013); https://doi.org/10.1155/2013/539312
22. J.A. Malek, *Thermochim. Acta*, **138**, 337 (1989); https://doi.org/10.1016/0040-6031(89)87270-3
23. J. Malek, *Thermochim. Acta*, **200**, 257 (1992); https://doi.org/10.1016/0040-6031(92)85118-F
24. T. Kanagasekaran, P. Mythili, P. Srinivasan, A.Y. Nooraldeen, P.K. Palanisamy and R. Gopalakrishnan, *Cryst. Growth Des.*, **8**, 2335 (2008); https://doi.org/10.1021/cg701132f
25. V. Fasano, J.E. Radcliffe and M.J. Ingleson, *Organometallics*, **36**, 1623 (2017); https://doi.org/10.1021/acs.organomet.7b00174
26. C. Sundararaja and S. Sagadevan, *Mater. Res.*, **21**, e20160595 (2018); https://doi.org/10.1590/1980-5373-MR-2016-0595